An innovative and low-cost system for in situ and real-time cure monitoring using electrical impedancemetry for thermoset and CFRP laminate

Huikangyue Bao, Philippe Marguerès, Philippe Olivier

Measurement Science and Technology

100 year anniversary
Measurement Science and Technology

ACCEPTED MANUSCRIPT

An innovative and low-cost system for in situ and real-time cure monitoring using electrical impedancemetry for thermoset and CFRP laminate.

To cite this article before publication: Huikangyue BAO *et al* 2023 *Meas. Sci. Technol.* in press https://doi.org/10.1088/1361-6501/ad14df

IOP Publishing Journal Title
Journal **XX** (XXXX) XXXXXX https://doi.org/XXXX/XXXX

An innovative and low-cost system for in situ and real-time cure monitoring using electrical impedancemetry for thermoset and CFRP laminate.

Huikangyue BAO[1], Philippe MARGUERÈS[1,*] and Philippe OLIVIER[1]

[1] Université de Toulouse, UT3, CNRS, Institut Clément Ader, 3 rue Caroline AIGLE - 31400 Toulouse, France

*Corresponding author, E-mail: philippe.margueres@iut-tlse3.fr

Received xxxxxx
Accepted for publication xxxxxx
Published xxxxxx

Abstract

This paper is divided into five sections. The first one introduces the context of our study dealing with the monitoring of the cure of structural composites made of carbon fibers and thermoset matrix (CFRP). The second one presents a brief state of the art. The third one deals with the materials characterized in this study, and the design and the production of a new bench dedicated to electrical impedance (EI) and thermal measurements. The fourth one compares the results obtained on CFRP and unreinforced matrix samples using conventional DSC and EI measurements. A conclusion and some prospectives close the paper.

In a recent previous work, we studied phases transitions in CFRP during their curing by EI showing that changes in the electrical complex impedance Z can easily be related to those of conventional parameters such as the thermoset matrix degree of cure α. This work was carried out using a commercial single-channel impedance analyzer: HIOKI. In addition to its high acquisition cost, this device presented certain limitations in terms of measurement channels (only one) and data acquisition rate (60s for a frequency sweep).

These facts led us to develop a new EI measurement bench for monitoring the impedance changes in CFRP part for aeronautical applications (airframe structures). The innovative new multi-channel (8) bench we designed and manufactured is based on the Digilent PmodIA module (never used previously for this purpose) and an Analog-Front-End (AFE) developed for EI measurements. It costs only 15% of the HIOKI analyzer and has a data acquisition rate 48 times higher (1,23 s versus 60 s). All this while maintaining an equivalent impedance measurement range: 100mΩ to 1MΩ.

The proposed approach makes it possible not only to monitor the degree of cure α (DOC), but also to detect potential cure cycle issues. This latter demonstration was carried out on a new composite material (vacuum-bag oven-cured), NC66/1808NA (supplied by CTMI), which, to our knowledge, had never been characterized in the literature. Compared with preliminary results, similar behavior is obtained on two different CFRPs using two different benches. This clearly underlines the value and quality of the study. Experimental validation of our approach will contribute to CFRP structural health monitoring (SHM).

Keywords: CFRP, Cure monitoring, Electrical Impedancemetry, material functionalization, smart material

1 Introduction

In the aeronautical industry, CFRP have been increasingly used owing to their high specific strength, stiffness, and ability to integrate multiple functionalities. The properties of composite structures depend on their manufacturing processes, especially during their cure cycle. Various cure monitoring techniques have been developed to improve the manufacturing reliability, reproducibility, and quality implementation. However, conventional cure monitoring techniques are limited by expensive measurement systems that use specific existing sensors or sensors developed for this purpose. Hence, a low-cost real-time cure monitoring method (EI) without additional sensors could be a preferential option to improve the CFRP manufacturing process.

Among the numerous online cure monitoring methods, dielectric analysis (DEA) is widely applied in aerospace, automotive, and electronics industries for quality control and process optimization. It involves applying a small AC voltage with variable frequency to the device under test and measuring the frequency response via local or bulk sensors. The cure behavior is determined by time-frequency analysis. However, DEA is commonly used to characterize glass fiber reinforced polymers (GFRP) or unreinforced matrix rather than CFRP, which has an anisotropic electrical response because of the presence and orientation of carbon fibers.

In this context, Marguerès et al. [1-5] focused on modelling the 3D anisotropic electrical conduction of CFRP structures and used electrical impedancemetry to analyze both low- and high-frequency components of electrical behavior during curing. This approach uses the material itself as a sensor (measurements using non-intrusive electrodes), which can be the key to the gateway of smart materials in the future. It is based on the correlation between the changes in rheological (such as storage modulus G,' loss modulus G", viscosity μ and loss factor tan δ) and the electrical impedance $\bar{Z}$ of CFRP which enables identifying the different physicochemical transition phases of polymerization. The cure behavior of CFRP is represented not only by the evolution of the modulus $\Delta|Z|$ and the argument $\Delta\theta$ over time but also by their first and second derivatives over time. This highlighted the feasibility of monitoring the 4 phase transitions of CFRP during curing: liquefaction, gelation, vitrification, and end of cure.

This preliminary approach has demonstrated the reliability of EI applied to CFRP cure monitoring. However, the bench, used in this previous work, was based on the specialized, high-accuracy, and monochannel impedance analyzer HIOKI 3570. The prohibitive cost of this instrument and numerous working environmental limits make it difficult to implement in industrial CFRP manufacturing. Against this backdrop, we have developed a low-cost, multichannel, and multiphysics bench, allowing this EI approach to be transferable from the academy to industry [6]. The new bench serves to monitor eight samples in electrical impedance changes and to measure temperature in oven at the same time, to adapt the four-wires measurement using an Analog-Front-End (AFE), and to detect any curing issues in real-time.

This paper is organized as follows. In Section 2, preliminary works are presented to highlight the originality of our approach. Section 3 introduces the samples and the experimental setup. Section 4 deals with the correlation between the cure monitoring results of DSC and EI, especially in the identification of critical points. In Section 5, main results are summarized, and some perspectives of our study are given.

2 Preliminary considerations

The purpose of our work is to link the physical-chemical transitions that unreinforced thermoset matrices and CFRP undergo during their curing to their global electrical behavior during this curing, by identifying several rheological critical points such as PL, PG, PV, and PF. Furthermore, our current work will enable us to understand the correlation between the changes in $\bar{Z}$ as a function of α knowing that changes in α themselves are determined by conventional thermal analysis and cure kinetics. This electrical-rheological-thermal correlation can serve to a multi-physics modelling of CFRP in the future. The preliminary consideration of our approach is about the thermal analysis and the cure monitoring methods with different sensors. Compared with these conventional techniques (see Section 2.1), EI method used for cure monitoring has numerous advantages that make it easier to be applied in CFRP manufacturing.

2.1 Thermal analysis of thermoset

Thermal analysis is a series of techniques used to understand the intrinsic properties of polymer, determine the thermal stability and decomposition behavior of the material. The results are useful for predicting performance and optimizing the cure cycle. Conventional thermal analysis techniques for thermoset polymers include Differential Scanning Calorimetry (DSC), Thermogravimetric Analysis (TGA), Dynamic Mechanical Analysis (DMA), Thermal Mechanical Analysis (TMA), please see Table 1.

Experimental methods	Measured parameters	Characteristics followed
DSC	Heat of Reaction (H, enthalpy)	Glass transition temperature Tg, degree of cure α, cure kinetics α=function (time, Temperature).
TGA	Mass	Thermal stability, filler content.

DMA	Complex, storage and loss moduli	Mech. manifestation of glass transition (temperature Tα), viscoelastic behavior, complex modulus.
TMA	Specific volume, CTE	Glass transition temperature, changes in material volume

Table 1. Measurement characteristics of different thermal analysis techniques.

Our methodology consists of comparing physicochemical results to EI results. It can be summarized as described in Figure 1. DSC is commonly used to determine the glass-transition temperature of polymer and its cure kinetic parameters using the reaction enthalpy [7-9]. In our study, the α determined by DSC is the key variable to link the electrical behavior with the physicochemical transitions of the thermoset matrix (unreinforced or in a carbon fiber composite).

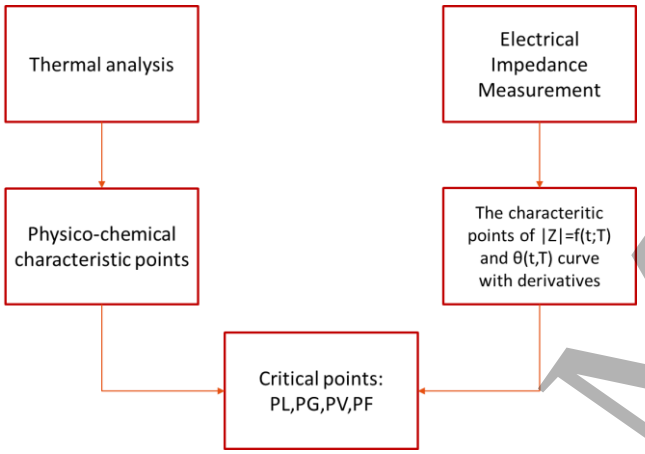

Figure 1. The logic diagram of cure monitoring using thermal analysis (DSC) and Physicochemical analysis (rheometer experiments) and in parallel electrical impedance real-time measured during cure cycles.

During a DSC scan, a sample is cured at a constant heat rate, at isothermal temperature or using a specific cure cycle. The heat flow $\phi=\frac{dQ}{dt}$ with Q the heat of reaction ($J.g^{-1}$), is measured by DSC. To determine the progress of the polymerization of the sample, the enthalpy H of the reaction is calculated as the integral of heat flux as a function of time (eq.1). The degree of cure as a function of the curing time α(t) is given by the ratio of H(t) to H_T (eq.2). H_T is the total enthalpy obtained for the complete polymerization of the thermoset resin.

$$H_T = \int_0^t \phi \, dt \qquad \text{eq. 1}$$

$$\alpha(t) = \frac{H(t)}{H_T} \qquad \text{eq. 2}$$

Regarding the cure kinetics of the polymeric matrix, the different critical points of polymerization can be determined by analyzing the changes in α during a cure cycle. The DSC results obtained with the unreinforced resin and with the carbon/epoxy prepreg can differ due to the presence of carbon fibers that exhibit a higher thermal conductivity than the one of polymeric resin and therefore modify the coefficient of thermal conductivity of the studied material (see §4).
The rheological critical points denoted by PL, PG, PV, and PF of the unreinforced resin epoxy M21 were determined owing to DSC et parallel-plate rheometer experiments clearly described in [10] (Figure 2 and Figure 8):

- PL corresponds to:
  - the minimum points of viscosity μ(t) and tanδ,
  - the onset point of α(t) located at the intersection point of the first and second asymptotes,
  - the first maximal value of the second derivative of the degree of cure with respect to time α" (t).
- PG corresponds to:
  - the major inflection point after PL of viscosity μ(t) and degree of cure α(t) (tending between 0.4 and 0.6 [9, 11-13])
  - the value of tanδ = 1,
  - the first minimal value of the second derivative of the degree of cure with respect to time α" (t).
- PF corresponds to:
  - the end of cross-linking and is related to the final maximum points of viscosity μ(t) and degree of cure α(t) (tending towards1),
  - a constant value of the conservative shear modulus G, loss shear modulus G" and tanδ.
- PV corresponds to:
  - the transition between the end of gelation (intersection point of the second and third asymptotes) and the end of cross-linking corresponding to PF (PF),
  - a local maximum of loss shear modulus G" and tanδ after the end of gelation,
  - α(t) tending between 0.9 and 0.95 [9, 13].

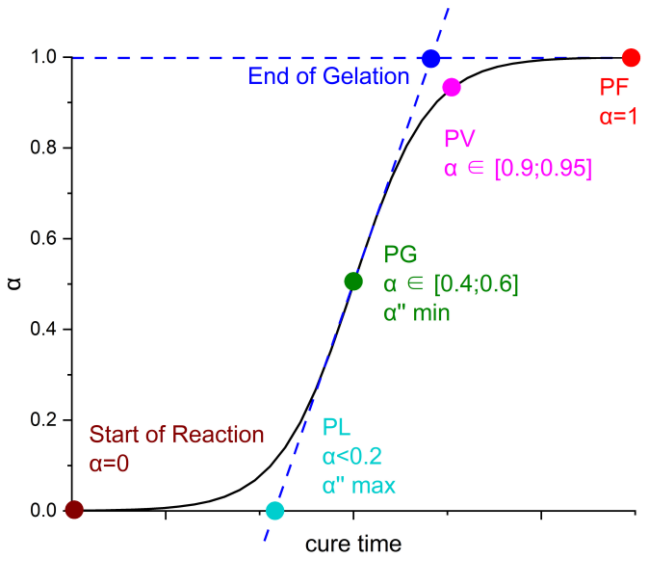

Figure 2. Identification of the critical physicochemical points PL, PG, PV, and PF of polymerization using the degree of cure curve α(t) for a complete polymerization

Results for unreinforced epoxy resin M21 [10] are given in Figure 8. Physicochemical behavior critical points PL, PG, PV, and PF are identified using the degree of cure α(t) curve. Two scales of time were used to give the times at which PL, PG, PV, and PF occur. The first scale is chronological cure time, while the second one takes the onset of isothermal dwell as origin of times. For example, this means that PL occurs 67 minutes after the beginning of the cure cycle or -6 minutes before the onset of the curing dwell at 180°C. Here the polymerization is not complete (due to the cure cycle), thus the α at PV is around 0.86 and at PF around 0.95.

2.2 Cure monitoring techniques and sensors

Since the 1970s, numerous experimental methods have been developed to monitor changes in a composite material, not only during curing but also under mechanical loading. For example, Bragg gratings (FBGs), ultrasonic or infrared sensors [14-18] are commonly used to monitor matrix phase changes during curing or to detect damage initiation or propagation. Electrical methods such as eddy current control [19-21] and piezoelectric sensors [22, 23] have been applied to structural health monitoring (SHM) by several authors.

Among these methods, DEA (dielectric analysis) is particularly valued in our research, because it serves to monitor the real-time cure of the polymer but also because it is based on the same physical principles as electrical impedance analysis (EI). The material under test is excited by a sweeping frequency AC electrical signal, and the information of the material is interpreted by the frequency analysis. The change in the complex dielectric permittivity $\bar{\varepsilon}$ of the polymer during curing is correlated with the physicochemical transition of the polymer, both the real part and the imaginary part are used to correlate rheological parameters as such the storage modulus G' and the loss modulus G." Furthermore, the dielectric loss factor δ considered as an analogy of the rheologic loss factor which is commonly used as an indicator of the phase changes in a progressing curing reaction.

Pantelelis et al. [24] proposed a polymerization monitoring method for thermoplastic using DEA sensors. In the purpose of identifying different transition phase, the point gelation PG and the end of cure PF are identified respectively by the inflection point and the final stabilization point in the dielectric behavior during curing.

Han et al. [25] have developed an approach of Electrochemical Impedance Spectroscopy to monitor resin cure processes using parallel-plate electrodes. The epoxy/amine system is modelled as a time-variant RC circuit which represents the difference between the initiation and the end of reaction. The α is calculated due to the changes in the electrochemical impedance measurement. The experimental data on the progress of cure is also validated by the comparison with the DSC results.

2.3 Preliminary results given by the EI method

The dielectric sensors are indispensable for the DEA but can be disrupted by interference from the electric field of carbon fibers. For this reason, most DEA techniques are applied to insulating materials such as unreinforced polymers or GFRP. To overcome the dependence on the dielectric sensor and apply it to carbon/epoxy composites, we have developed a new EI method using CFRPs themselves as sensors for polymerization control and SHM. As with the DEA technique, EI is based on the frequency analysis of complex electrical impedance $\bar{Z}$, which contains the resistive information about the carbon fibers in the real part, and the capacitive information about the resin in the imaginary part. The modulus |Z| and the argument θ are calculated from two parts.

The CFRP structure exhibits anisotropic properties, including electrical conductivity. Carbon fibers exhibit pure resistivity in the longitudinal direction. On the contrary, conduction in the transverse direction (intraply or through the thickness) is based on percolation theory [2-5, 26]. Consequently, conductivity in the transverse direction depends on inter-fiber contacts and fiber volume fraction. The inter-fibers contact points created by the fiber waviness are modelled as resistors, whereas the resin in the adjacent area is modelled as a capacitor.

The passage of electric current in the transverse direction is ensured by the 3D percolation network of resistors and capacitors. Consequently, a homogeneous conduction model of the CFRP structure, composed of numerous parallel RC circuits, has been developed. The relationship between the function of $\bar{Z}$ and the equivalent RC circuit of the model is illustrated by the following equations (eq. 3 to 5).

$$\bar{Z}=\frac{R}{1+j\omega RC} \qquad \text{eq. 3}$$

$$|Z|=\frac{R}{\sqrt{1+\omega^2R^2C^2}} \qquad \text{eq. 4}$$

$$\theta=-\arctan(\omega RC) \qquad \text{eq. 5}$$

Where: ω (rad/s) is the signal pulse with ω=2πf (Hz); R the resistance (Ω) and C the capacitance (F) of the material; j, an imaginary number such as $j^2=-1$.

As part of preliminary research, CFRP laminates (manufactured from T700/M21 carbon/epoxy prepreg) were real-time monitored, during their polymerization in oven or autoclave, using a bench including the Hioki IM3570 impedance analyzer (https://www.hioki.com/). The samples were continuously excited by a sinusoidal sweep signal and polymerization behaviors were observed using time functions such as |Z|=f(t) and θ=f(t).

Preliminary results have demonstrated the feasibility of monitoring reaction progress and detecting cure issues by the EI method. Critical points such as PL, PG, PV, and PF are determined using electrical impedance measurements exhibiting globally the same shape of behavior in the longitudinal, transverse or through-the-thickness directions (Table 2). From the reference signatures, vacuum leaks at critical points during curing were clearly highlighted by an abnormal EI behavior (Figure 9) [27].

Critical Points	**|Z|**	**θ**
PL	Local minimum	Local maximum
PG	Local maximum	Local minimum
PV		Local maximum
PF		Local maximum

Table 2. Critical points correlated to EI transverse measurements on T700/M21 samples.

In our previous works several stacking sequences were studied (with 8, 16 and 32 plies):

- unidirectional samples: $[0°_8]$, $[0°_{16}]$ and $[0°_{32}]$;
- quasi-isotropic samples: $[0°/+45°/-45°/0°]_s$, $[0°/+45°/-45°/0°]_{2s}$ and $[0°/+45°/-45°/0°]_{4s}$.

The global tendencies of electrical responses (the equivalent parallel resistance in the through-the-thickness direction R_{pz}) of the QI (quasi-isotropic) and the UD (unidirectional) samples are similar. An example is given in Figure 3 for $[0°_{16}]$, $[0°_{32}]$, , $[0°/+45°/-45°/0°]_{2s}$ and $[0°/+45°/-45°/0°]_{4s}$ oven-cured samples. For QI samples the electrical conductivity is enhanced compared to unidirectional samples. This could be linked to a better percolation network.

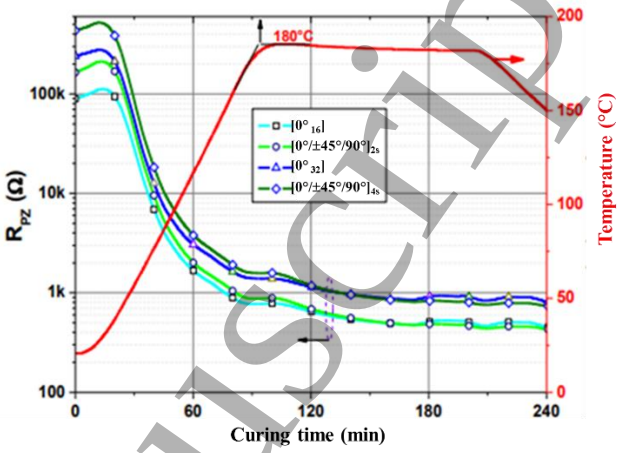

Figure 3. Comparison between **UD and QI** samples during curing [10].

Furthermore, two types of electrodes were compared [4;26]: a copper tape (135 µm with passivation; 3M 1181 Tape copper film and Kapton High Temperature Masking Tape Multicomp film) and a copper mesh (CUA1 Copper Metallic Cloth Annealed No. 162.44 FR 0.050, Gantois).

From a microstructural point of view, the performance analyses have not shown any defect (e.g., porosity, delamination, etc.) in the area of the copper mesh after manufacturing of samples. This is not the case when using plain copper tapes which produce a hindrance in resin flows during curing and generates local porosities.

Furthermore, mechanical tests (tensile, flexural and ILSS tests) were carried out to highlight potential intrusive effects. These tests showed that the copper mesh electrodes had no harmful effect, unlike the ones using plain copper tape. This led to choose only electrodes made of copper mesh.

Several thousands of aircraft equipped with composite wings are currently flying with thousands of square meters of copper mesh embedded just beneath the surface of composites parts [31-34].

The work presented here is based on the same approach but using a new homemade low-cost bench which is only 15% of the cost of the previous measurement bench (with Hioki). The samples studied are CFRP laminates made from NC66/NA1808 prepregs and unreinforced NA1808 matrix samples, to highlight differences in behavior and the effect of carbon fibers.

It can be said that the EI method applied to cure monitoring exhibits the following advantages:

- The CFRP material is used as its own sensor (self-sensing and no intrusive).
- The method does not induce significant changes in the overall manufacturing process.
- The copper mesh electrode remaining in the CFRP structure can be used for SHM purpose or for active NDE (InfraRed thermography for example) or de-icing in the aeronautics field (wing leading edges).

The total cost of the measurement system is only 15% compared with the previous bench using Hioki impedance analyzer.

3 Experimental setup

This section presents the samples and the experimental setup. A series of DSC and EI experiments have been accomplished. Our approach is based on the following assumption: under the same cure conditions (time and temperature), the arrival time at the characteristic points of α for the different samples is consistent. DSC measurements on prepregs and unreinforced matrix were performed for this purpose and compared with EI measurements.

Experimental equipment used in this work is as follows:

- A homemade bench (it will be described later in this paper);
- An impedance analyser (Hioki IM3570, https://www.hioki.com/);
- An 8-channel thermocouple data logger (PicoLog TC-08, https://www.picotech.com/);
- A curing oven (MPC) equipped with a vacuum pump;
- A DSC (Q50-TA instrument, https://www.tainstruments.com/).

Samples made of unreinforced NA1808 resin (approximate mass: 1 g) and unidirectional eight plies [0°$_8$] and sixteen plies [0°$_{16}$] laminates (10 x10 cm² samples) made of NC66/NA1808 prepreg (matrix mass fraction W_m=35%) were oven-cured (vacuum bag only) with the same cure cycle (Figure 4 and Figure 5):

- Heating rate: 2°C/min from room temperature to 120°C,
- Isothermal dwell: 120°C, 90 min,
- Vacuum: -700 mbar.

Figure 4. Experimental setup in the oven with unidirectional laminates under vacuum bag (VBO vacuum bag only process).

Samples made of NA1808 unreinforced resin (approximate mass: 7 mg) and NC66/NA1808 prepregs (approximate mass: 20mg) were used to characterize the degree of cure α and the rate of reaction $\frac{d\alpha}{dt}$ using a Q50-TA Instruments DSC.DSC data were used to build cure kinetics based on Kamal-Sourour modelling [28].

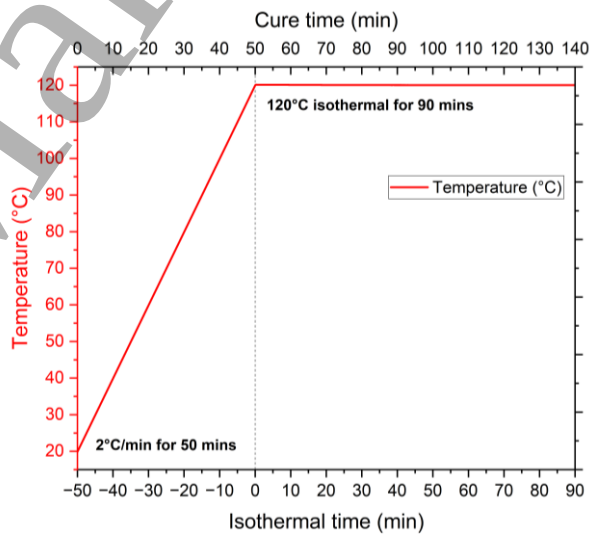

Figure 5. Oven cure cycle for NA1808 resin and NC66/NA1808 prepregs.

3.1 Materials

CFRP laminates are made of NC66/NA1808 prepregs (supplied by CTMI France https://www.ctmi.fr/en/aeronautics-8, see Table 3). Samples are 10 x 10 cm² square unidirectional plates: 2 mm-thick [0°$_8$] and 4 mm-thick [0°$_{16}$] laminates.

Thin, flexible copper fabric electrodes (100-µm thick) - supplied by Gantois Industries- are embedded between chosen plies in CFRP laminates, according to different

configurations, to ensure current flow in different measurement directions: L (longitudinal), T (transverse), DL (diagonal-through-the-thickness-longitudinal) and DT (diagonal-through-the-thickness-transverse). In the L and T configurations, two electrodes are inserted horizontally into the inter-ply between the two highest plies of the laminate. In the DT and DL configurations, the first electrode is inserted between the two highest plies, and the second is inserted between the two lowest plies. These configurations are shown in Figure 10.

Marguerès et al. [30] have demonstrated the equivalence between diagonal thickness and through-the-thickness direction EI measurements and the non-intrusiveness effect of copper fabric electrodes. After curing, the electrodes remain in the CFRP laminates for further structural health monitoring (SHM) purpose.

Unreinforced matrix samples are made as follows (Figure 6). NA1808 was placed on a 10 mm × 10 mm × 2 mm silicone rubber frame. Frames are sealed with an insulating adhesive whose dielectric constant is significantly higher than that of the resin, ensuring that the sample will not be short-circuited during high-frequency electrical excitation. Two identical electrodes are placed on the top and bottom surfaces of the resin sample.

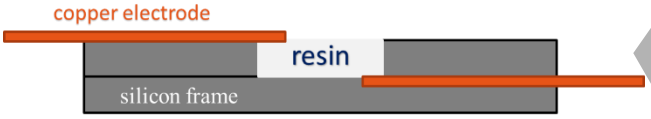

Figure 6. Unreinforced matrix samples in silicone-rubber frame

Overall, there are totally 19 [0°$_8$] samples, 9 [0°$_{16}$] samples and 8 unreinforced resins samples cured in the oven and monitored by EI system in the 4 cycles. For each cycle, there are 8 samples monitored by the homemade bench and 1 sample monitored by Hioki IM3570 for the purpose of comparison. The information given by the samples is shown in the Table 4. The different electrodes configurations of NC66/NA1808 laminate samples are highlighted. All the unreinforced resin NA1808 samples are measured in the DT (diagonal-transverse) configuration as shown in Figure 10.

3.2 Measurement bench

A new homemade bench has been developed. It proposes eight channels for EI measurements and two channels for temperature measurements (Figure 7-a). EI measurements are carried out with eight PmodIA (PmodIA datasheet: https://digilent.com/reference/pmod/pmodia/start) impedance analyzers and a multiplexer (MUX). The samples are excited by a sinusoidal sweep voltage and the instantaneous response in |Z| and θ is calculated and converted to a digital signal. A data acquisition board (DAQ) is used for transmission from the bench to the PC.

The samples, in the oven, are connected to the bench using HiFi wires, with a resistance lower than 0.01Ω and an inductance lower than 1x10^{-5} H. Connection between the HiFi wires and the copper electrodes is made by soldering. Open-circuit and short-circuit experiments were performed (at room temperature and during curing) to measure the parasitic elements (compensated during measurement) and to demonstrate that the wired system does not have a thermal response. The short-circuit impedance of the system is around 4.6 Ω, and impedances below this value will be distorted.

The accuracy of the new bench was evaluated by measurements on T700/M21 cured samples. To validate the new bench, the Hioki IM3570 was used in continuous acquisition mode for comparison purposes during curing. Based on the results of preliminary studies, the proposed scanning frequency range is 5 kHz to 50 kHz with a 5 kHz step, including the optimal frequency F=10 kHz for the T700/M21. The data acquisition time in an EI channel is approximately 1.23 s, which guarantees the accuracy of the first- and second-time derivatives of |Z| and θ.

To validate the accuracy of thermal measurements, a PicoLog module (www.picotech.com) was used to measure temperature during curing via several thermocouples. Thermocouples, linked to the bench and to the PicoLog module, are placed next to the laminates under the vacuum bagging film.

To ensure longitudinal EI measurements, a specific analogue front end (AFE) has been developed to enable four-wire measurements with PmodIA (Figure 7-b.). The results obtained with and without AFE will be discussed in the next section.

4 Results and Discussion

4.1 Identification of critical points by DSC

In this fourth section, the different physicochemical transition phases of five samples made with NC66/NA1808 prepreg and 5 samples made with unreinforced NA1808 resin are identified by the changes in degree of cure α measured by DSC. PL, PG, PV, and PF points are determined as explained in §2.1 and are given in Table. **5**. Globally, results are similar, the time differences between each critical point for unreinforced resin and prepregs are linked to the presence of carbon fibers and the changes that they induce in material conductivity. For all samples, the polymerization is not complete (due to the cure cycle). For unreinforced resin samples, the maximal α reaches 90% and, for prepreg samples, it reaches 85%. Thus, α values at PG and at PV are lower than

samples undergoing a complete polymerization (with α reaching 100% at the end of cure).

4.2 Identification of the cure critical points by EI

This section presents the results of cure monitoring using EI for CFRP and unreinforced resin samples. Changes in |Z| and θ for CFRP [0°$_8$] laminates will be discussed first. Next, results in the longitudinal (L) direction will be outlined and the AFE value discussed. The results for unreinforced resin will then be compared with those for CFRP samples to highlight the effect of the presence of carbon fibers. Finally, all identified critical points will be compared with the DSC results.

4.2.1 NC66/NA1808 [0°$_8$] samples – Transverse through the thickness measurements

The laminate samples are submitted to a sweep frequency from 5 kHz to 50 kHz with a peak-to-peak voltage (Vpp=0.84 V). Figure 11 shows the changes in |Z| and θ measurements at different frequencies during curing, only the results of five extracted frequencies (10 kHz, 20 kHz, 30 kHz, 40 kHz, and 50 kHz) are presented. The |Z| curves overlap, while the θ curves remain globally parallel with values tending towards 0° at the end of curing. The [0°$_8$] samples are almost purely resistive in the thickness direction, certainly due to an extensive percolation network. Furthermore, θ curves are inverses of |Z| curves exhibiting same extrema points in time regardless of frequency. The high fiber content (65%) in NC66/1808NA samples may explain this phenomenon. The results obtained on the T700/M21 samples (fiber content equal to 51%), used in previous works, were more dependent on frequency.

To validate the trend of measurements obtained with the new bench, measurements were also taken for 2 same cure cycles (C1 and C2) using the Hioki impedance analyzer. An example of results is given in Figure 12. Results trends are similar for all the [0°$_8$] samples using both benches.

Based on changes in |Z| and θ during curing on NC66/NA1808 samples, PL and PG are identified by a local minimum and maximum of |Z| respectively (Figure 13). PV and PF are identified using θ measurements (Figure 13) but also using the first- and second-time derivatives of |Z| (Figure 14). After PG, the |Z| curve can be divided into three stages: a dynamic part, a damping part, and a stationary part. PV is the transition point between the first two parts (clearly visible on |Z|' curve and with a local minimum of |Z|"). PF is the transition point between the last two parts with values of |Z|' and Z|" tending towards 0.

When comparing the results given by the EI measurements and cure critical point detection for NC66/1808NA using the new bench, with those obtained for T700/M21 samples using the previous bench based on Hioki IM3570 (Figure 15), the trends obtained are identical. This confirms that our approach and our new homemade low-cost bench could yield typical signatures with CFRPs.

4.2.2 NC66/NA1808 [0°$_8$] samples – Longitudinal through the thickness measurements

To ensure the accuracy of longitudinal measurements on CFRP laminates, EI 4-point measurements are required. To provide a 4-point configuration on the new bench, an AFE was developed to complement the capabilities of PmodIA, which can initially only provide 2-point measurements. It consists of two parts: a current source and an instrumentation amplifier (INA). The signal in voltage is converted to a current which excites the samples. Furthermore, the voltage across samples is measured by an instrumentation amplifier and sent to the bench. The parasite elements of wires are thus eliminated because of the separation of the excitation source and the measurement device.

Figure 16 gives longitudinal measurements obtained on NC66/NA1808 [0°$_8$] samples using PmodIA without (PmodIA-L-UD8) and with AFE (AFE-L-UD8). The result obtained using PmodIA is distorted by the parasitic impedance of the system (around 4.6Ω). On the contrary, AFE can measure small impedances (<1Ω) with greater sensitivity. Although the |Z| value measured by PmodIA is not correct, the overall behavior is like that using AFE. Thus, critical points can also be identified using PmodIA in the longitudinal direction. The key to monitor the cure cycle using EI measurements lies not in the value of |Z| but in its changes and variation Δ|Z|.

All critical points can be detected using |Z| and |Z|' as shown in Figure 17: PV is correlated to a local maximum of |Z|' and PF to the last local maximum of |Z|'.

4.2.3 NA1808 unreinforced resin samples

Unlike CFRP laminates, unreinforced resin samples exhibit isotropic behavior when excited by a sweep frequency voltage, and their response in |Z| and θ is frequency-dependent (Figure 18).

Unreinforced resin is an insulating material with charge carrier enabling ionic conduction. At the end of the liquefaction phase, the resin reaches the minimum viscosity and the maximum ionic conductivity, so PL correlates with the main peak that corresponds to the minimum of |Z| and the maximum of θ, respectively. The resin exhibits a high capacity before and after PL because dipolar rotation predominates over ionic conduction, so that θ tends towards - 90°. After PL, θ curve can be divided into two stages: a dynamic part and a more global stationary part. PG can be identified as the transition point between these two parts and therefore can be found using the asymptotic method (Figure 19). In the more stationary part, two slight transitions can be detected on the θ curve using |Z|' and θ.' These two local transitions can be

associated with PV and PF (Figure 20). These points can be detected on all samples and at all frequencies.

4.2.4 Results comparison

Results obtained by EI and DSC are given in Table 6. The results of the EI are the average of multiple samples from different cure cycles. All the critical points could be identified by EI method, with globally good agreement with DSC results. Results gaps (mostly for PL and PG) could be linked to the presence of carbon fibers (between prepreg and unreinforced resin samples), and mass effect (between EI and DSC samples). The effect of thermal inertia in the cure cycle (curing oven with 1 m^3 volume and DSC with only a few milligram samples) can also lead to some discrepancies.

4.3 Cure issues detection by EI

In this section, the idea is to show how various issues occurring during the cure of a composite laminate can be detected only owing to impedancemetry. The detectability of defects during curing is studied using two different tests. In the first test, it was decided to see if a lack of vacuum can be detected, while in the second one a break in the power supply of the cure cycle for a few minutes inducing a few minutes stop of the curing oven heating resistances was simulated.

For the lack of vacuum testing, a CFRP [$0°_8$] sample was placed outside the vacuum bag. Changes in |Z|=f(t) at 10 kHz in the DT direction were measured and compared to those of another [$0°_8$] placed inside the vacuum bag during the same cure cycle (Figure 21). Both samples have the same initial |Z| value at the beginning of cure. The absence of vacuum significantly affects the overall cure behavior in |Z|, particularly before the vitrification phase. It shows a completely different behavior of |Z| in the liquefaction phase, certainly due to a lack of resin flow and a worse carbon-fiber-percolation network. At the end of the cure, the final |Z| value is almost twice the normal value. PL and PG cannot be detected as usual and after crossing the PV, the |Z| trend of the two laminates began to converge until the end of the cure. The |Z|' curves of the two samples are given to highlight this in Figure 22.

For the break in the cure cycle, the cure cycle was interrupted 14 minutes before the isotherm dwell arrival time for 4 minutes and then restarted. Two different stacking sequences were used for the purpose: [$0°_8$] and [$0°_{16}$] samples. As shown in Figure 23, the break induced a time delay for PL and PG. From a general point of view, interrupting curing before the PG does not alter the overall behavior of the |Z| curve and does not cause abnormal values but simply results in a time delay.

Table 7 gives the obtained PL and PG for the samples shown in Figure 23. Obviously, a delay of about 60s is obtained for [$0°_8$] samples and about 80s for [$0°_{16}$] samples.

In conclusion, both the lack of vacuum and the cure interruption can be detected by the proposed EI approach.

5 Conclusion and perspectives

In this paper, we have proposed a specific approach, based on electrical impedancemetry (EI), to ensure cure monitoring of CFRP using a new, low-cost homemade bench, using PmodIA analyzers, developed for this purpose. Different samples (few mg) made of NC66/NA1808 prepreg and NA1808 unreinforced resin were used to highlight physicochemical transitions in the resin polymerization during a specific cure cycle. Up to four critical points were identified to allow comparison with the EI approach: the liquefaction point (PL), the gelation point (PG), the vitrification point (PV) and the end of reaction (PF). CFRP laminates (around 100cm^2) and unreinforced resin sample (around 1g) were oven cured and EI measurements were performed using the same cure cycle. Copper mesh electrodes were used to access the material used here as a sensor in its own state, without any significant changes in the overall manufacturing process. EI results were analyzed considering changes in impedance modulus |Z| and argument θ, considering local and global information given by first- and second-time derivatives, and asymptotic approach. Obtained results highlight a good agreement in the definition of PL, PG, PV, and PF, using the EI methodology. Some discrepancies were observed between the DSC and EI samples but also between prepregs and unreinforced resin samples. This could be linked to the presence of carbon fibers, mass effect and cycle inertia.

Global trends of the presented results are also in good agreement with previous ones obtained on T700/M21 samples using a first bench using a Hioki IM3570 analyzer. This enables us to think that the proposed approach could yield typical signatures with CFRPs, which could ease cure monitoring. Furthermore, the feasibility to detect faults during curing was demonstrated using two different tests: a lack of vacuum and a break in the cure cycle for a few minutes during curing. A completely different EI signature was obtained in the first case, and a shift in time was highlighted in the second one.

As the copper mesh used as electrodes can remain in the CFRP structure, the proposed approach can be used for in service monitoring to address SHM purpose. Moreover, as the material is instrumented with electrodes, it can be used for active NDE (infrared tomography) and de-icing for example. Thus, to complete our approach of the EI methodology applied in SHM, an optimized thermal-electrical-mechanical modelling would be developed as part of a more in-depth study. A virtual material will be designed to describe the material changes not only during curing but also during mechanical loading. In addition, the experimental and

numerical results will be discussed in a case of good agreement and an inverse approach could be proposed for material and process optimization purposes.

References

[1] P. Marguerès, T. Camps, and P. Olivier, 2014 *Revue des composites et des matériaux avancés*, **24**, 207-220, doi: 10.3166/rcma.24.207-220.

[2] S. Sassi, P. Marguerès, T. Camps, M. Mounkaila and P. Olivier, 2015 *e-Journal of Nondestructive Testing* **20** (2). https://www.ndt.net/?id=17074

[3] M. Mounkaila, T. Camps, S. Sassi, P. Marguerès, P. Olivier, C. Escriba and J. Fourniols. 2015 *e-Journal of Nondestructive Testing* **20** (2) https://www.ndt.net/?id=17073

[4] S. Sassi, P. Marguerès, P. Olivier, and R. Le Begue, 2016 *Composites Part A: Applied Science and Manufacturing*, **80**, 204-216, doi: 10.1016/j.compositesa.2015.10.022.

[5] M. Mounkaila *et al.*, 2018. *Smart Materials and Structures*, **27**, 085004. doi: 10.1088/1361-665X/aacdba.

[6] H. Bao, P. Marguerès, and P. Olivier, 2023 In: *Proceedings of European Workshop on Structural Health Monitoring (EWSHM)*, **1**, P. Rizzo and A. Milazzo, Eds. Springer Cham International Publishing, 816-825. doi: https://doi.org/10.1007/978-3-031-07322-9

[7] R. Hardis, J.L.P. Jessop, F.E. Peters, and M.R. Kessler, 2013 *Composites Part A: Applied Science and Manufacturing*, **49**, 100-108, doi: 10.1016/j.compositesa.2013.01.021.

[8] Y. Zhang, R. Fang, H. Xue, J. Xia, and Q. Lin, 2022 *Thermochimica Acta*, **711**, 179210, doi: https://doi.org/10.1016/j.tca.2022.179210.

[9] S.S. Hwang, S.Y. Park, G.-C. Kwon, and W.J. Choi, *The International Journal of Advanced Manufacturing Technology*, **99**, no. 9, pp. 2743-2753, 2018/12/01 2018, doi: 10.1007/s00170-018-2467-y.

[10] M. Mounkaila, 2016 *Ph.D. Thesis, Universite Toulouse III Paul Sabatier, 26/04/2016*. https://hal.laas.fr/tel-01813627v1/document.

[11] N. Zobeiry, A. Poursartip, 2015 In: *Structural Integrity and Durability of Advanced Composites*, P.W.R. Beaumont, C. Soutis, and A. Hodzic Eds. Woodhead Publishing, 43-72.

[12] I. Baran, K. Cinar, N. Ersoy, R. Akkerman, and J.H. Hattel, 2017 *Archives of Computational Methods in Engineering*, **24**, 365-395, doi: 10.1007/s11831-016-9167-2.

[13] C. Li, N. Zobeiry, K. Keil, S. Chatterjee, and A. Poursartip, 2014 In: *Proceedings of International SAMPE Technical Conference*, 10-11 March 2014 Paris. https://www.proceedings.com/38477.html

[14] M. Mulle, F. Collombet, P. Olivier, and Y.H. Grunevald, 2009 *Composites Part A: Applied Science and Manufacturing*, **40**, 94-104, doi: 10.1016/j.compositesa.2008.10.008.

[15] M. Mulle *et al.*, 2009 *Composites Part A: Applied Science and Manufacturing*, **40**, 1534-1544, doi: 10.1016/j.compositesa.2009.06.013.

[16] S.I.. Takeda, Y. Aoki, and Y. Nagao, 2012 *Composite Structures*, **94**, 813-819, doi: 10.1016/j.compstruct.2011.02.020.

[17] C. Garnier, M.L. Pastor, F. Eyma, and B. Lorrain, 2011 *Composite Structures*, **93**, 1328-1336, doi: 10.1016/j.compstruct.2010.10.017.

[18] Z. Zhang, M. Liu, Q. Li, and Y. Ang, 2020 *Composites Communications*, **22**, doi: 10.1016/j.coco.2020.100435.

[19] H. Menana and M. Feliachi, 2009 *IEEE Transactions on Magnetics*, **45**, 1008-1011, doi: 10.1109/tmag.2009.2012542.

[20] K. Mizukami, Y. Mizutani, A. Todoroki, and Y. Suzuki, 2016 *Composites Part B: Engineering*, **86**, 84-94, doi: 10.1016/j.compositesb.2015.09.041.

[21] X. Xu, H. Ji, J. Qiu, J. Cheng, Y. Wu, and T. Takagi, 2018 *NDT & E International*, **94**, 79-91, doi: 10.1016/j.ndteint.2017.12.003.

[22] D. Wang and D. D. L. Chung, *Carbon*, **60**, 129-138, 2013, doi: 10.1016/j.carbon.2013.04.005.

[23] Y. Yu, X. Liu, X. Cui, Y. Wang, and X. Qing, *Composites Science and Technology*, **240**, 110079, doi: https://doi.org/10.1016/j.compscitech.2023.110079.

[24] N. Pantelelis, G. Maistros, and C. Hakme, 2007 *International SAMPE Symposium and Exhibition (Proceedings)*. 52.

[25] Y. Han, J. Wang, H. Zhang, S. Zhao, Q. Ma, and Z. Wang, *Sensors and Actuators A: Physical*, **250**, 78-86, doi: https://doi.org/10.1016/j.sna.2016.08.028.

[26] S. Sassi, 2016 *Ph.D. thesis, Université Toulouse III Paul Sabatier*, 2016. https://www.theses.fr/2016TOU30070.

[27] P. Margueres, P. Olivier, M. Mounkaila, S. Sassi, and T. Camps, 2020 *International Journal of Smart and Nano Materials*, **11**, 417-430, doi: 10.1080/19475411.2020.1843559.

[28] M.R. Kamal and S. Sourour, 1973 *Polymer Engineering & Science*, **13**, 59-64, doi: https://doi.org/10.1002/pen.760130110.

[29] A.T. Le, P. Olivier, Q. Govignon, A. Sangar, P. Boulanger, et al. 2019 *JNC 21 : Journées Nationales sur les Composites (Proceedings)*

[30] P. Margueres, T. Camps, M. Viargues, and P. Olivier, 2013 *Measurement Science and Technology*, **24**, 095005, doi: https://doi.org/10.1088/0957-0233/24/9/095005.7

[31] S. Black, 2013, *Composites World*, https://www.compositesworld.com/articles/lightning-strike-protection-strategies-for-composite-aircraft. Accessed Nov. 15 2023

[32] G. Woodrum, G., 1970, *SAE Technical Paper 700935*, , https://doi.org/10.4271/700935.

[32] H. Kawakami and P. Feraboli, 2011, Composites Part A: Applied Science and Manufacturing, **42**, 1247-1262, https://doi.org/10.1016/j.compositesa.2011.05.007.

[33] T.M. Dhanya and C.S. Yerramalli, 2018, *Materials Today Communications*, **16**, 124-134, https://doi.org/10.1016/j.mtcomm.2018.05.009.

[34] GSweers, B. Birch and J. Gokcen, 2012, *Aero Magazine*, **QTR_04.12**,18-28,https://www.boeing.com/commercial/aeromagazine/articles/2012_q4/4/. Accessed Nov. 15 2023

Figures and Tables for which size cannot be reduced to the width of a single column.

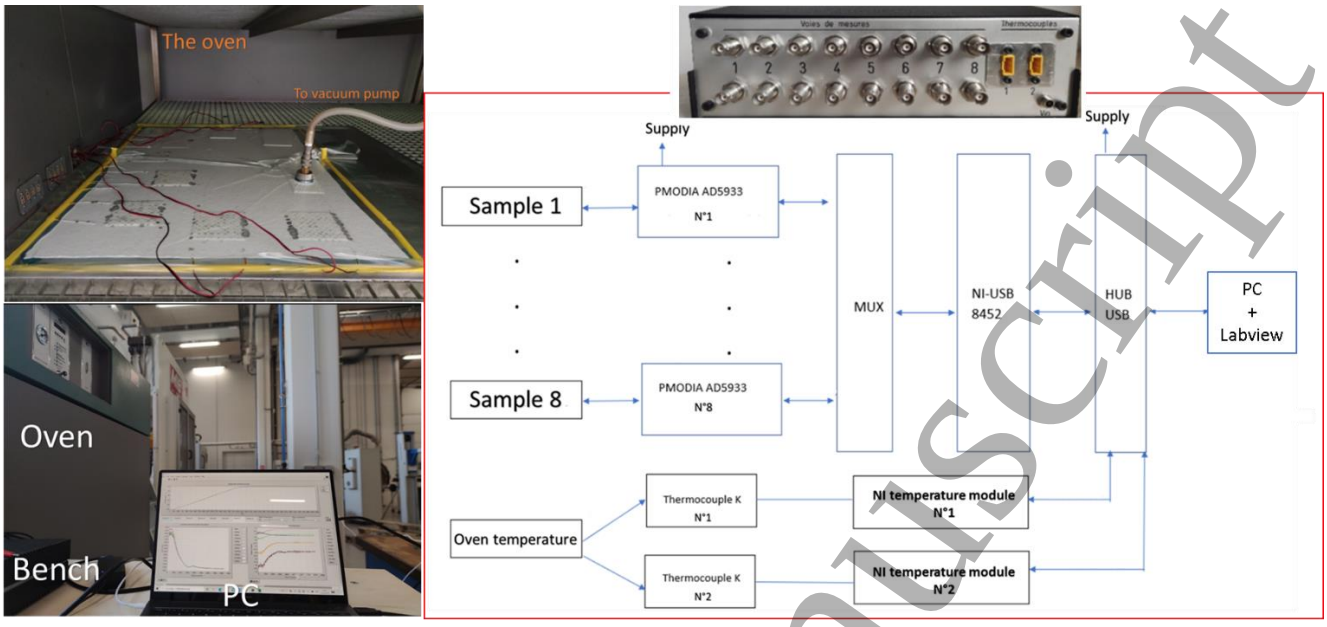

a

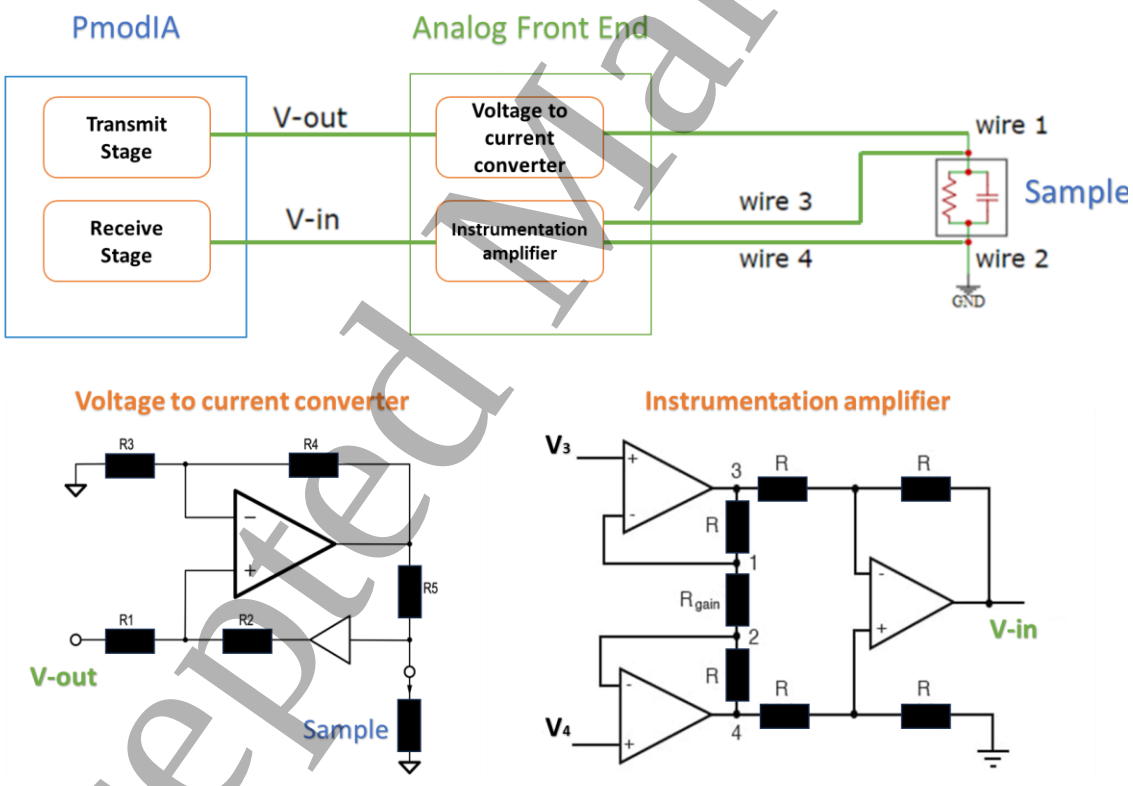

b

Figure 7. a- Device implementation of the new bench and CFRP cure monitoring in an oven (see PmodIA schematic here: https://digilent.com/reference/_media/reference/pmod/pmodia/pmodia_sch.pdf . Accessed nov 15 2023); b- Analog Front End (AFE) schematic. This AFE can be connected optionally between the PmodIA and the sample for 4-point EI measurements.

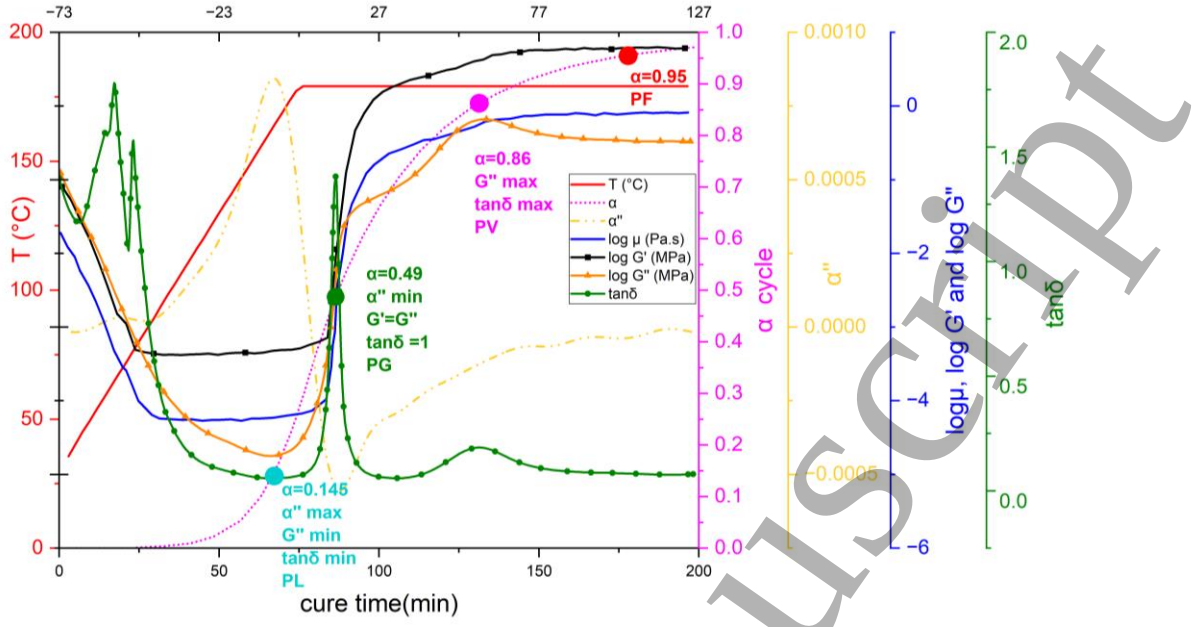

Figure 8. Chemo-rheological behavior of the unreinforced M21 epoxy resin during the heating ramp and the curing dwell of the manufacturer-recommended cure cycle. Changes in α, its second time derivative α'', viscosity μ, shear moduli (storage) G' and (loss) G'' and tanδ as functions of time. Locations of rheological critical points (PL, PG, PV, and PF) of the unreinforced resin epoxy M21. On the top of figure are given characteristic times at which PL, PG, PV, and PF are located. These times are calculated from the origin of times (written in red) and from the origin of the curing dwell isotherm (written in black).

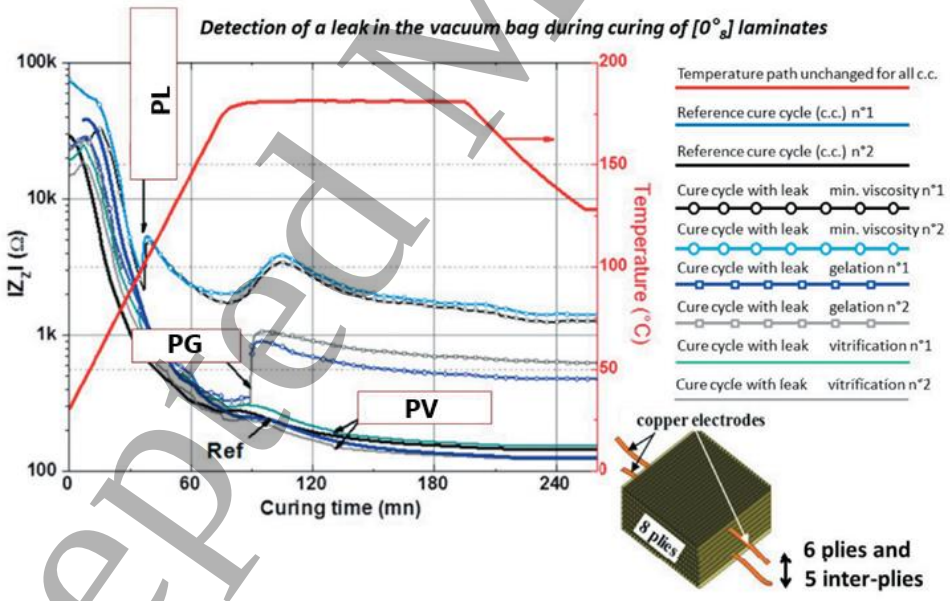

Figure 9. Using EI response to detect leaks in the vacuum bag during curing of a T700/M21 [0°8] laminate [27]. Four different cure cycles (repeated twice for reliability) were compared: the reference cure cycle (recommended by prepreg manufacturer); cure cycles with leaks in vacuum bag occurring at PL, PG and PV.

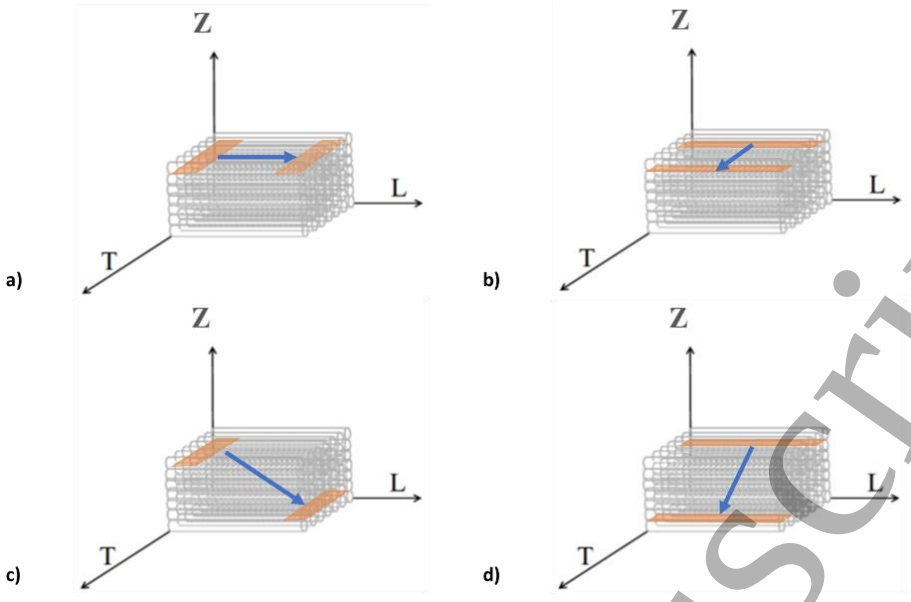

Figure 10. The different electrodes (orange rectangles) configurations with the current flow (blue arrows). (a): L (longitudinal), (b): T (transverse), (c): DL (diagonal-through-the-thickness-longitudinal) and (d): DT (diagonal-through-the-thickness-transverse).

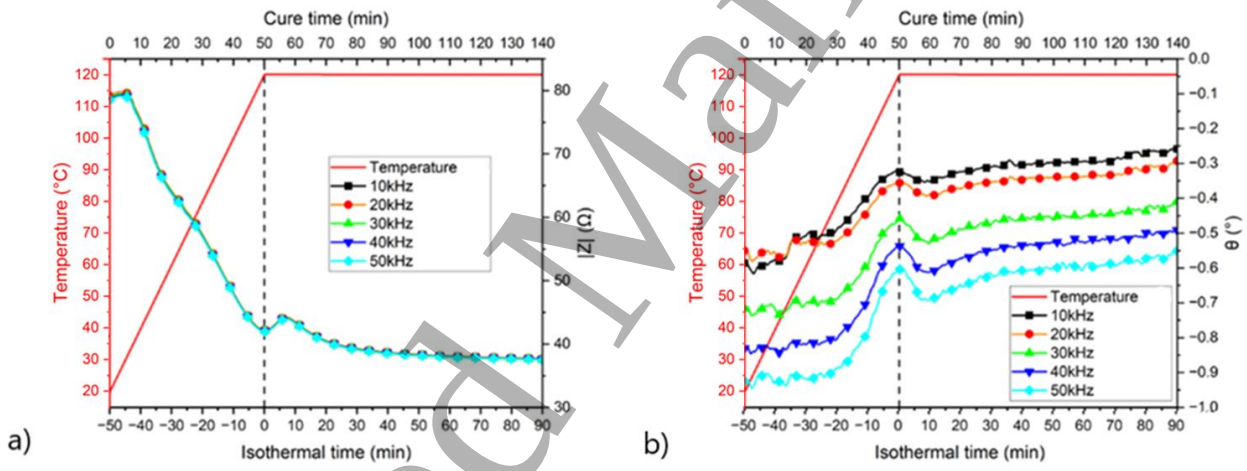

Figure 11. The frequency response in (a) |Z| and (b) θ of the $[0°_8]$ in DT direction.

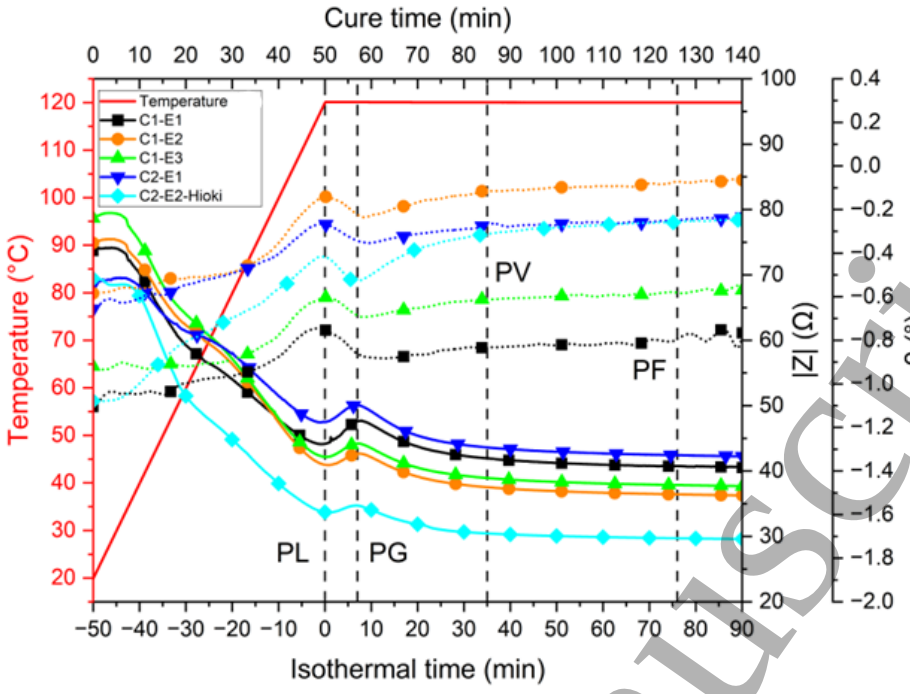

Figure 12. |Z| (solid lines) and θ (dashed lines) of [0°$_8$] samples at10 kHz using the new homemade bench and Hioki impedance analyzer, for two different cure cycles denoted by C1 (3 samples tested and indicated E1, E2 and E3) and C2 (2 samples tested and indicated E1 and E2).

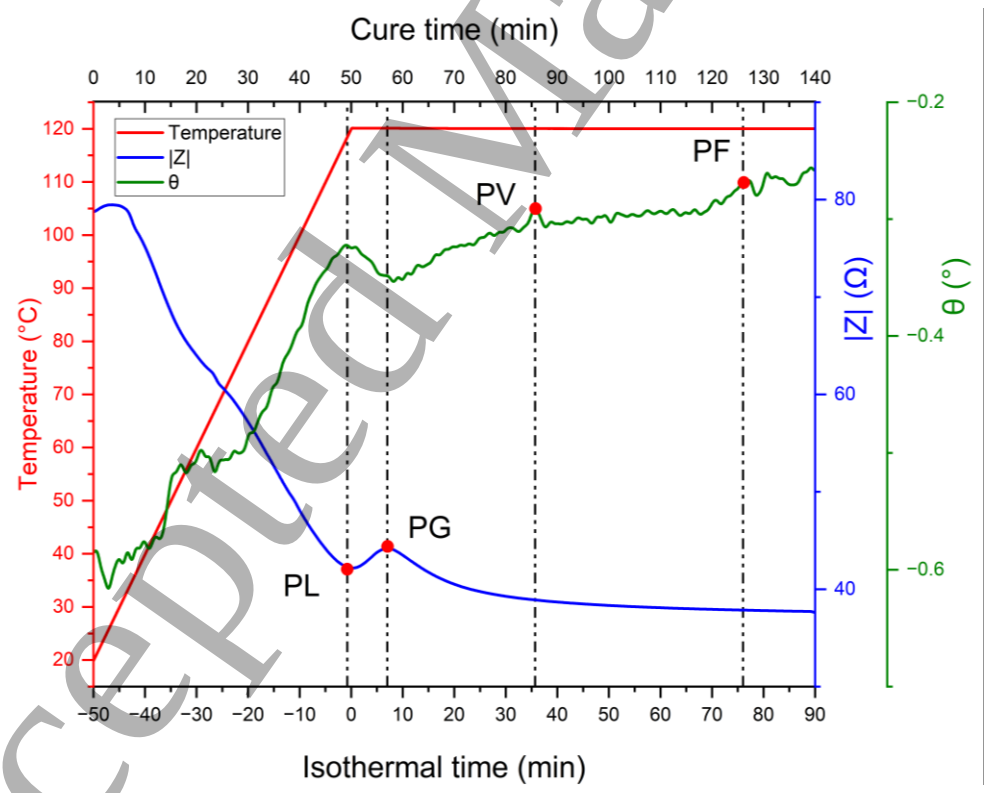

Figure 13. The critical points PL, PG, PV, and PF identified by EI on NC66/NA1808 [0°$_8$] samples.

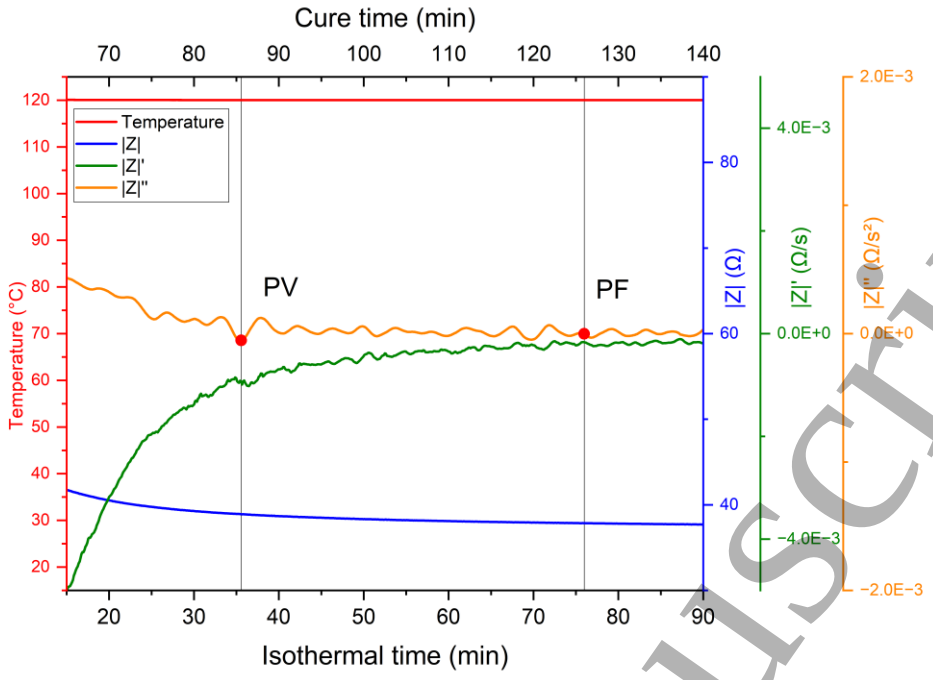

Figure 14. PV and PF identified using |Z|' and |Z|'' for of NC66/NA1808 [0°$_8$] samples.

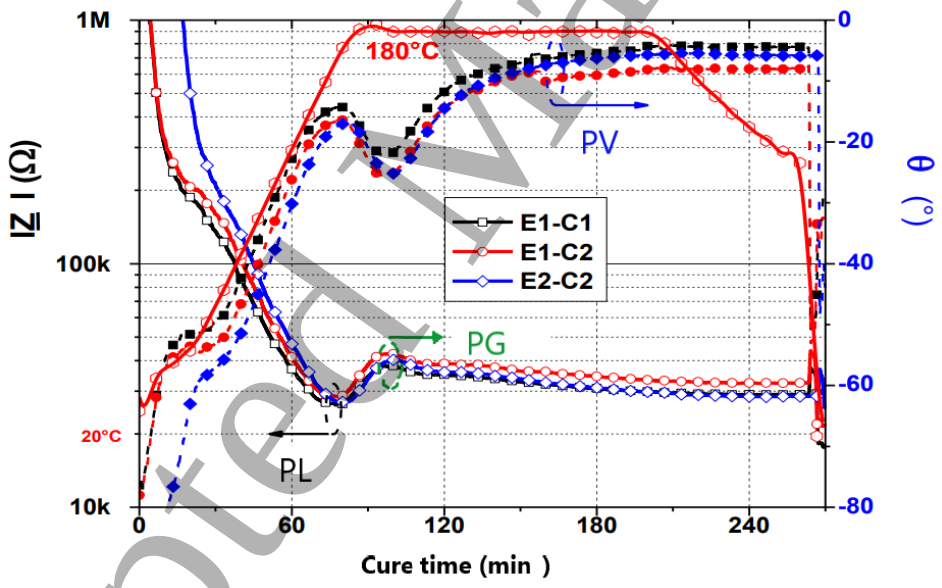

Figure 15. |Z| and θ measurements for T700/M21 samples at 10 kHz obtained using Hioki IM3570, for two different cure sets (C1 with one sample indicated E1 and C2 with two samples indicated E1 and E2).

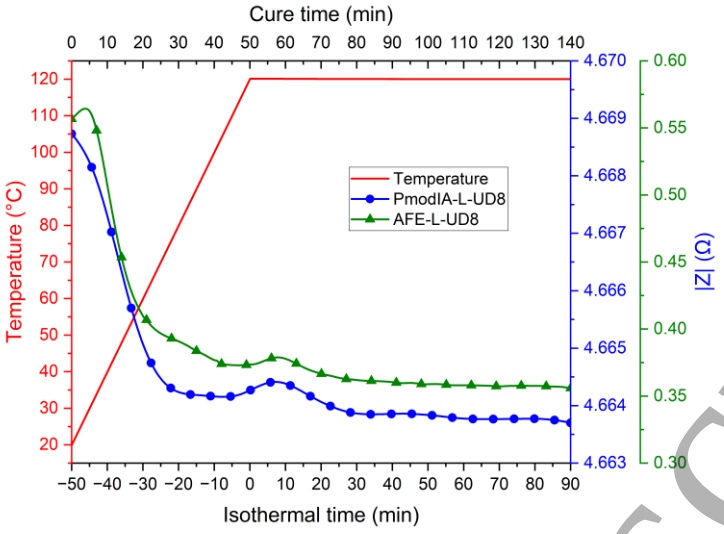

Figure 16. Longitudinal results using PmodIA and AFE at 10 kHz on NC66/NA1808 [0°$_8$] samples.

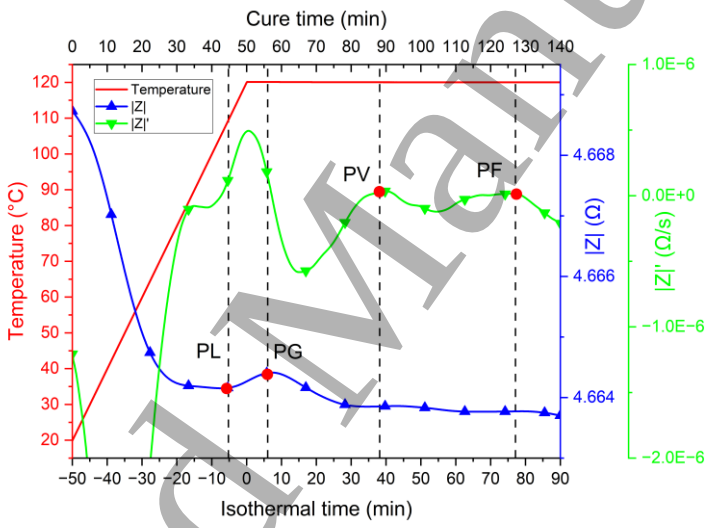

Figure 17. Longitudinal |Z| and |Z|' measurements at 10 kHz on NC66/NA1808 [0°8] samples

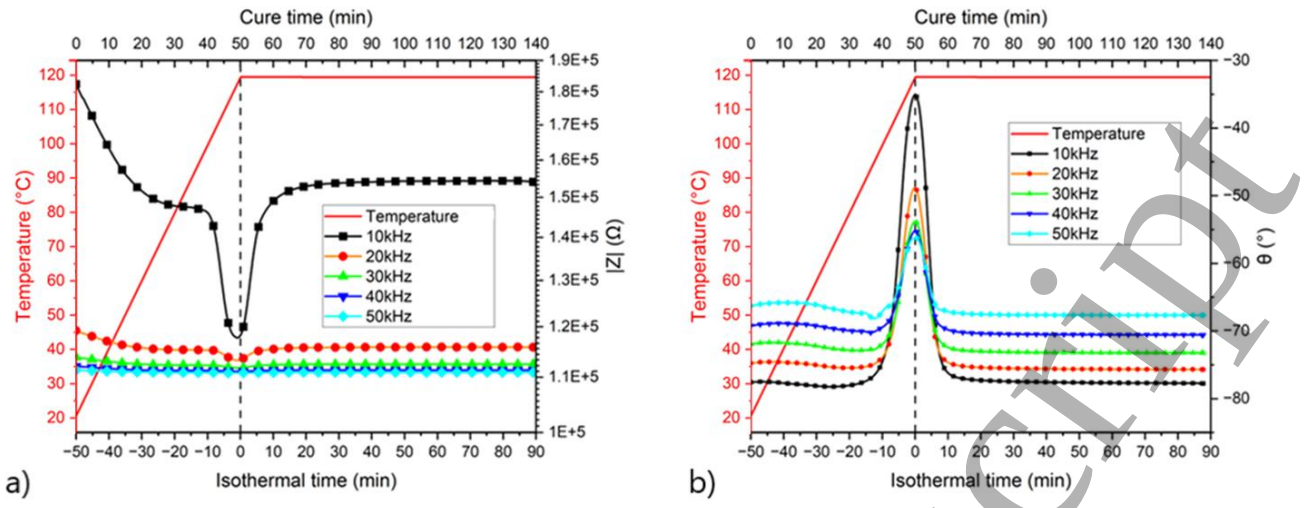

Figure 18. (a) the frequency response in |Z| and (b) θ for unreinforced resin samples.

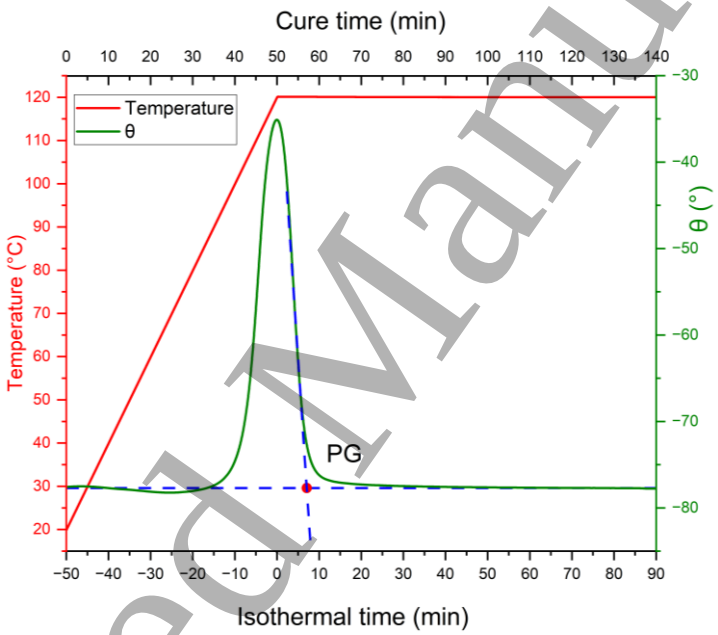

Figure 19. Gel point PG of the unreinforced NA1808 resin obtained using the asymptotic method on θ=f(t) at f=10 kHz

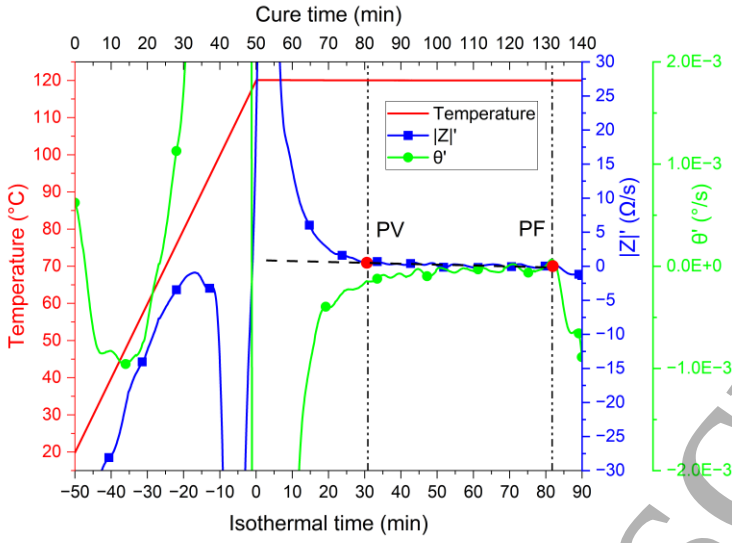

Figure 20. Identification of the vitrification point (PV) and the end of cure point (PF) using |Z|' and θ' for unreinforced resin samples at f= 10 kHz.

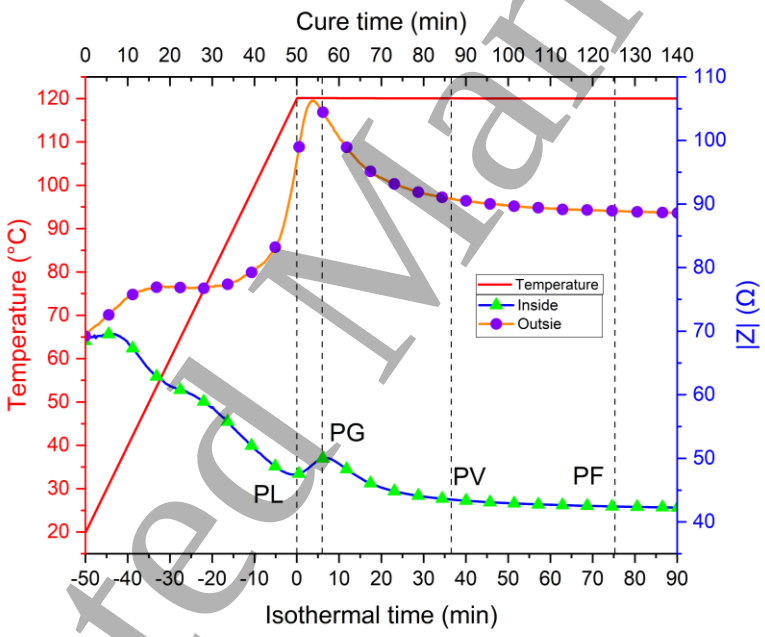

Figure 21. |Z| measurement in CFRP [0°$_8$] samples placed outside and inside the vacuum bag during the same cure cycle.

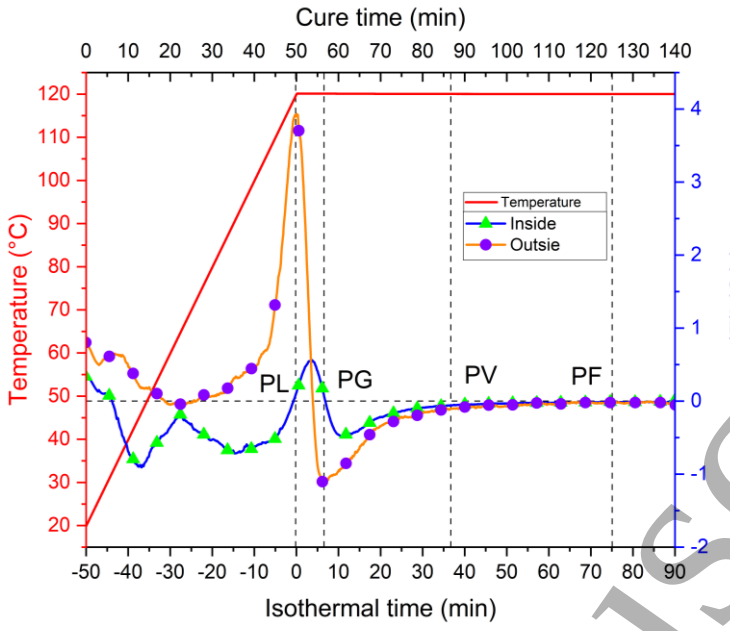

Figure 22. |Z|' measurement on CFRP [0°$_8$] samples placed outside and inside the vacuum bag during the same cure cycle.

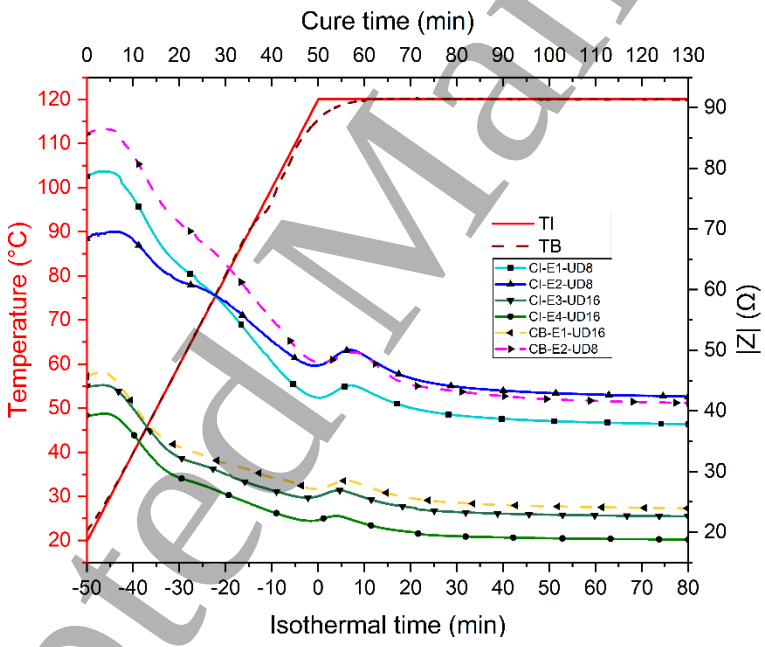

Figure 23. Comparison of |Z| measurements for normal cycles (CI, with 3 samples tested and indicated E1, E2 and E3) and a cycle with 4 minutes power supply breakage (CB, with 2 samples tested and indicated E1 and E2) at 10 kHz, with normal oven temperature TI and broken temperature CB (breakage in power supply).

Carbon fiber NC66	**Resin NA1808 (cured)**	**Prepreg NC66/NA1808**
Diameter:7µm Conductivity: 10^5 S/m	Density: 1.18g/cm^3 Tg:128°C Viscosity at 80°C: 5Pa.s	Ply thickness: 125 µm Fiber volume fraction: 61±3.5% Orientation of fibers: UD

Table 3. NC66 carbon fibers, NA1808 epoxy system and NC66/NA1808 prepreg data [29].

Cure cycles (See Fig. 6)	**NC66/NA1808 [0°$_8$]**	**NC66/NA1808 [0°$_{16}$]**	**Unreinforced resin NA1808**	**The samples monitored by Hioki IM3570**
1st cure cycle (C1)	2L, 2T, 2DL, 2DT	0	0	[0°$_8$] DT
2nd	2DT	2DL, 2DT	2	[0°$_8$] DT
3rd	2DT, 2DL	2DT	2	[0°$_{16}$] DT
4th cure cycle (C4)	2DT, 1DL	2DT	3	Unreinforced resin

Table 4. Set of tests performed. Curing conditions were kept constant. Four oven-curing were carried out. The table gives electrodes configuration (see Fig.7).

	NC66/NA1808 prepreg		NA1808 resin	
Critical points	**α (%)**	**Isothermal time (min)**	**α (%)**	**Isothermal time (min)**
PL	7.0±0.5	-0.70±0.11	8.0±0.4	-0.63±0.04
PG	36.4±1.4	7.16±0.33	38.9±1.2	6.06±0.06
PV	79.5±1.1	35.55±0.72	84.0±0.9	35.66±0.20
PF	85.0±1.5	78.00±0.23	90.0±1.0	81.03±0.27

Table. 5 PL, PG, PV, and PF with isothermal time in minutes deduced from the DSC analysis.

Critical points	**Laminate EI (min)**	**Laminate DSC (min)**	**Resin EI (min)**	**Resin DSC (min)**
PL	-0.25±0.06 s	-0.70±0.11	-1.28±0.04 s	-0.63±0.04
PG	6.91±0.05 s	7.16±0.33	6.00±0.6 s	6.06±0.06
PV	36.88±0.63 s	35.55±0.72	36.10±0.33 s	35.66±0.20
PF	76.13±0.71 s	78.00±0.23	82.50±0.46 s	81.03±.0.27

Table 6. Comparison between critical points (with isothermal time in minutes) obtained by EI with those classically determined by DSC and rheology measurements.

Samples	**PL (isothermal time)**	**PG (isothermal time)**
CI [0°$_8$]	-18s	430s
CB [0°$_8$]	41s	484s
CI [0°$_{16}$]	-95s	270s
CB [0°$_{16}$]	-15s	360s

Table 7. Obtained low viscosity points PL and gel points PG for [0°$_8$] and [0°$_{16}$] samples cured with normal and abnormal cycles (4 min of break).